A high sensitivity magnetic sensor based on the evanescent scattering by a magnetorheological film

BINGHUI LI, [1] HAU PING CHAN,[1]* KAZI TANVIR AHMMED, [1,2] LIANGJUN HE, [1] SHUYAN ZHU, [1] AND QIANG WU[3]

[1]*Department of Electrical Engineering, City University of Hong Kong, 83 Tat Chee Avenue, Kowloon Tong, Hong Kong*
[2]*Department of Electrical and Electronic Engineering, University of Chittagong, Chittagong-4331, Bangladesh*
[3]*Department of Mathematics, Physics, and Electrical Engineering, Northumbria University, Newcastle upon Tyne NE1 8ST, U.K.*
**Corresponding author: eehpchan@cityu.edu.hk*

Received XX Month XXXX; revised XX Month, XXXX; accepted XX Month XXXX; posted XX Month XXXX (Doc. ID XXXXX); published XX Month XXXX

We present a simple concept to implement a magnetic sensor that uses evanescent scattering by a suspended magnetorheological (MR) film above a planar waveguide. The soft MR film embedded with ferromagnetic particles is to induce scattering on the evanescent field of a planar waveguide at a proximity distance. This distance can be controlled precisely by a magnetic field. Consequently, the waveguide output power changes in response to the magnetic intensity. Two sensor prototypes of different film thickness were designed and tested showing a tradeoff between the sensitivity and dynamic sensing range. A maximum sensitivity of ~2.62 dB/mT was obtained. Compared with optical MEMS, the presented sensors feature simple design, easy fabrication, low cost and potentials of large-scale production and miniaturization to be integrated into portable devices.

http://dx.doi.org/10.1364/OL.99.099999

For decades, magnetic sensors have been aiding mankind throughout modern technology in various fields, including satellite attitude control, electric current monitoring, and magnetic resonance imaging (MRI) etc. [1]. For most applications, optical magnetic sensors (OMS) have been attracting more attentions in recent years, since OMS offer reliable, noninvasive detections, while exhibiting advantages of lightweight, compact size, and high adaptability in harsh environments in where surround by toxicity, high moisture, or high electromagnetic interferences. High performance OMS with sub-*p*T resolution [2], like optically pumped magnetometers (OPMs), are weak either in dynamic sensing range or demand stringent cooling / shielding apparatus. On the contrary, OMS based on an optical waveguide feature in lightweight design as well as small footprint and are emerging as considerable candidates for magnetic sensing. The principle can be mainly classified as intrinsic or extrinsic Faraday rotation sensors (FRS) [3,4] and evanescent coupling sensors. Intrinsic FRS detect the rotation of light polarizations after passing through an optical fiber [3]. The sensor demands a sub-meter scale sensing length due to low Verdet-constant of silica fibers. Extrinsic FRS shrink the sensing footprint using high Verdet-constant materials. However, it suffers from complex micro-fabrications and high building cost [4]. Evanescent coupling sensors employ magnetic susceptible ferrofluid as the waveguide cladding by incorporating of various optical structures such as interferometers and optical gratings etc. [5-7]. These sensors own high design flexibility, however, suffer from huge material scattering loss. As a result, ferrofluid need to be diluted before injecting into waveguide. The dilution procedure reduces its field susceptibility, adds design complexity and raises the cost since non-volatile solvent of proper refractive index is needed. Moreover, ferrofluid entails drawbacks of low saturation magnetization and short lifetime due to its liquid form.

Towards high sensitivity and compact size, optical micro-electromechanical systems (MEMS) sensors have been studied in recent years. One example refers to generate a Lorentz force onto a current carrying microcantilever, which in turn creates bending to be interrogated by microscopic imaging or fibers buddle [8,9]. However, optical MEMS desire complex micromachining techniques and high building cost, while most of them are difficult to realize large-scale productions in the industrial manufacturing. In addition, the signal interrogations are weak either in limited sensitivity or microscope resolution. The current carried in the coil should not be high to prevent from temperature fluctuations. To circumvent these drawbacks, in this Letter, we propose to replace the current-carrying cantilever by a magnetorheological (MR) film. The MR film, which is embedded with ferromagnetic particles, will be stimulated by the magnetic torque to form micro bending. In the meantime, we employ the principle of evanescent wave scattering (EWS) for interrogations [10,11]. By doing so, these drawbacks of optical MEMS sensors can be circumvented by two aspects: 1) MR film shows high susceptibility to the magnetic field, thereby offering capability of sensing weak magnetic field; (2) Temperature fluctuations were suppressed since no electricity appears in the setup. To facilitate the evanescent scattering, the MR

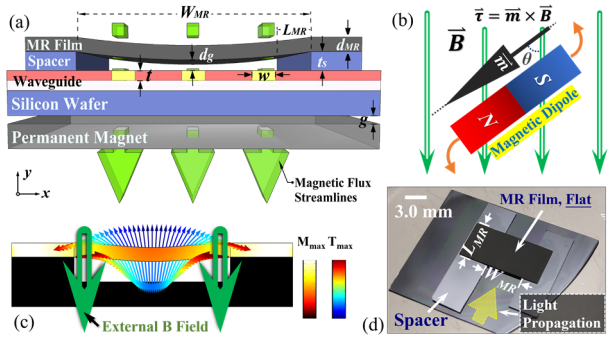

Fig. 1. (a) Schematic diagram of proposed EWS magnetic sensor; (b) Sensing principle of magnetic torque of a magnetic dipole; (c) Simulated Maxwell stress tensor *T* (arrows) on MR film surfaces; (d) Fabricated sample before dropping index matching liquid.

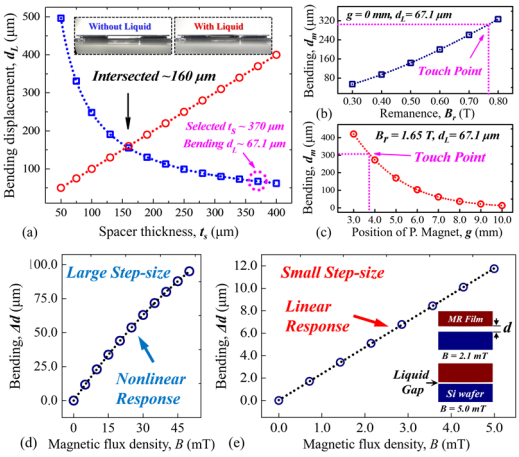

Fig. 2. (a) Bending displacement d_L versus spacer thickness t_s (blue: bending displacement d_L; red: a linear expression of t_s). (b) Bending displacement d_m versus magnetic remanence B_r at g=0 mm. (c) Bending displacement d_m versus gap distancer g at B_r=1.65 T. Liquid surface tension γ=0.037N/m, MR film Modulus E=2.73 MPa. Simulated bending Δd by magnetic field of large step-size (d) from 0 to 50 mT and small step-size (e) from 0 to 5.0 mT.

film was carefully suspended above a planar waveguide by a pair of spacers. A permanent magnet (PM) was positioned beneath the waveguide to pre-bias the MR film into the evanescent field. Afterwards, the magnetic field will stimulate the micro bending to the MR film, which induces scattering loss on the propagating wave at a proximity distance. This distance can be controlled by a magnetic field. Consequently, the waveguide output power changes in response to the magnetic intensity.

Figure 1(a) illustrates the front view of proposed EWS platform, for depicting the sensing principle. The MR film (width W_{MR}, length L_{MR}, thickness d_{MR}) was prepared by mixing ferromagnetic microparticles (BASF CIP-CS, 6.0–7.0 μm in diameter) with the PDMS matrix and subsequent thermal curing. The MR film was suspended on top of a liquid-cladded waveguide (core width w, core thickness t) by a pair of spacers (thickness t_s, central gap distance d_g). The permanent magnet (PM, beneath the waveguide with a space g) here serves two functions: 1) it generates a magnetic gradient force to pre-bias the MR film into the evanescent field; 2) it produces initial magnetization to the MR film for subsequent actuation. To facilitate the film bending, an external magnetic field (green arrow) imposes vertical (y-axis) magnetic flux onto the MR film, thereby bringing magnetic torques which tend to bend the film to align with the magnetic direction. Figure 1(b) depicts an example to illustrate the actuation principle, wherein a magnetic dipole with magnetic moments m (black arrow) was placed in a background magnetic field B (green arrow). The magnetic torque τ received by the magnetic dipole, can be expressed by the equation [1]: $\tau = m \times B$. Given by the initial conditions in Figure 1(b), this equation indicates that the magnetic torque will rotate the dipole anticlockwise toward an alignment which is parallel to the B field. However, reversal either direction of B or m will lead to a reversal of the dipole's rotation direction. That features our platform an advantage that it can distinguish the magnetic polarity in real time. Since m is generated by the PM, the magnetization direction of the PM is a key factor that determines the sensing performance. To make the analysis simple, we classify the sensor design as two alignments, i.e. Positive alignment and Negative alignment. The magnetic field B and PM remanence B_r exhibit the same field directions in the case of Positive alignment, while they are opposite in Negative alignment. If we negelect the material loss, the waveguide output power P_{out} can be expressed as $P_{out} = P_{in} - P_{scat}$, where P_{in} and P_{scat} refer to the input and scattered light power, respectively. Since P_{scat} depends on d, while d can be controlled by B. As a result, by monitoring P_{out}, the B field intensity and its polarity can be easily interrogated by referring to P_{out}.

The commercial Comsol Multiphysics was to simulate and predict the behavior of the sensor. In Figure 1(c), we simulate the generated magnetization (M) inside the MR film by the PM at B_r =1.65 T. The magnetization appears stronger on sides of the MR film, while lower in its center section due to non-uniform magnetization by the PM. We also simulate the Maxwell stress tensor T on the upper and lower surfaces of MR film under a Positive alignment, as depicted by arrows in Figure 1(c). The arrows of T depict the bending orientation for each MR film surface. However, the equivalent bending of MR film relies on the stress difference between the upper and lower surfaces. In Positive alignment (Figure 1c), MR film bends downward to the waveguide surface to boost light scattering. While in Negative alignment, the magnetic dipole tends to align horizontally, which brings the MR film away from the waveguide. To facilitate the evanescent scattering, an index matching liquid was filled into the gap between MR film and the waveguide. Figure 1(d) shows the fabricated sample, in which the size of sensing region is designed as $W_{MR} \times L_{MR} \cong 5.0 \times 5.0$ mm^2 at the spacer thickness t_s~370 μm. The dimension can be further reduced to suit various application.

To generate evanescent scattering, a pre-bending is necessary to bias the MR thin film into the evanescent field. In our study, pre-bending is achieved by two approaches (gravitation is negligible in our case), i.e. magnetic gradient bending d_m by the PM and the surface tension (γ) bending d_L by the liquid in the gap. From Figure 1(a), we define that $d_g = t_s - (d_L + d_m)$. By imposing a surface stress on film lower surface [12,13], $P = \gamma / t_s$, Figure 2(a) simulates the bending d_L versus the spacer thickness t_s for d_{MR}=210 μm. It is expected that the bending d_L is very sensitive to d_{MR}. In our design, the thickness of MR film d_{MR} was designed at sub-millimeter scale to ensure enough support. However, it can be reduced by choosing other materials to improve its stiffness. With a decrease of gap distance, the surface stress exerted on MR surface would be strengthened, which indicates that d_L grows as reducing the spacer thickness t_s (blue line). However in the case of t_s ~160 μm, d_L is equal to t_s (red line), and d_g=0, which indicates that the MR film will

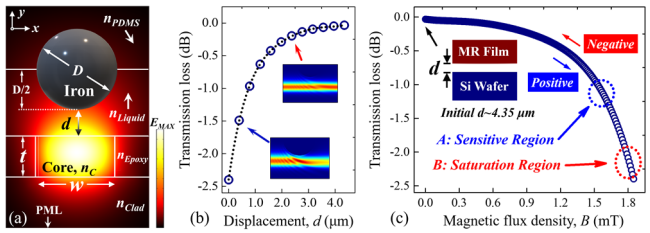

Fig. 3. (a) Simulation by FDTD solutions, n_C=1.573, n_{Clad}=1.541, n_{PDMS} =1.400, n_{Epoxy}=1.565, n_{Liquid}=1.557, w=5 μm and t=2.3 μm (b) Simulated transmission loss by a single iron particle (c) Correlated transmission loss versus the external magnetic flux density B at initial d=4.35μm.

physically touch the waveguide surface. To avoid this, we chose silicon wafer as the spacer due to its secure thickness of t_s~370 μm. In this case the induced bending d_L was ~67.1 μm. In Figure 2(a) inset, we compare the microscopic images of MR films before and after filling the liquid, wherein a clear micro-bending was visable with the liquid. Moreover, under an initial d_L = 67.1 μm, we simulate and compare the PM induced pre-bending d_m versus the remanance B_r and space distance g shown in Figures 2(b) and 2(c), respectively. Results reveal that, by either increasing B_r or reducing g, the MR film tends to bend close to the waveguide surface. Same as liquid tension, magnetic biasings can also let the MR film touch the waveguide. In the experiment, the pre-biasing of MR film can be done in two ways, i.e. to tune g at a fixed B_r , or to regulate B_r by a strong electromagnet at a fixed g. In this Letter, we chose former one with a PM at B_r=1.65 T to simplify the operation.

Given that t_s = 370 μm, B_r =1.65 T and g = 3.85 mm, the MR film (relative permeability ~1.985) was simulated to be pre-biased to d_g~4.35 μm as depicted from Figure 2(c). In this case, the MR film will be close enough to interact with the evanescent field. Figure 2(d) presents the simulated MR film bending displacement Δd induced by an external magnetic field B in Positive alignment. The magnetic field range is set to be 50 mT and 5.0 mT, in Figures 2(d) and 2(e), respectively. The results reveal a nonlinear bending Δd at a large step-size of magnetic field B as indicated by Figure 2(d). However, in the case of smaller step-size, i.e. 0-5 mT in Figure 2(e), the response turns to be highly linear with a sensitivity of ~2.4 μm/mT. Since the evanescent field is mostly dominant in a range of sub-10 μm, the dynamic sensing range for the sensor would be in a range of ~5 mT. This sensing range would be flexibly tuned by choosing suitable MR film materials and geometrical designs.

The simulated evanescent scattering loss by a single iron particle was depicted in Figure 3, with all parameter settings listed in the caption. The particle (D=7.0 μm) filled into PDMS matrix (n_{PDMS}) locates above a liquid-cladded optical waveguide (core n_C, lower cladding n_{Clad}) at a gap distance d. The PDMS matrix can be partially etched by a reactive ion etching (RIE) process, which is defined as D/2 shown in Figure 3(a). Figure 3(b) presents the simulated scattering loss by a single particle by tuning d from 0 to ~4.5 μm, in which a maximum loss ~2.5 dB can be achieved. In addition, the scattering loss shows a nonlinear behavior. In Figure 3(c), we correlate the transmission loss versus the magnetic flux density B at an initial d = 4.35 μm. It also depicts a nonlinear response. To point out, the result presents two special regions labelled in Figure 3(c), i.e. Sensitive region A and Saturation region B. Region around A depicts high sensitivity and therefore it is suitable for sensing. While for the region around B, the MR film will be physically touching the waveguide surface to prevent from

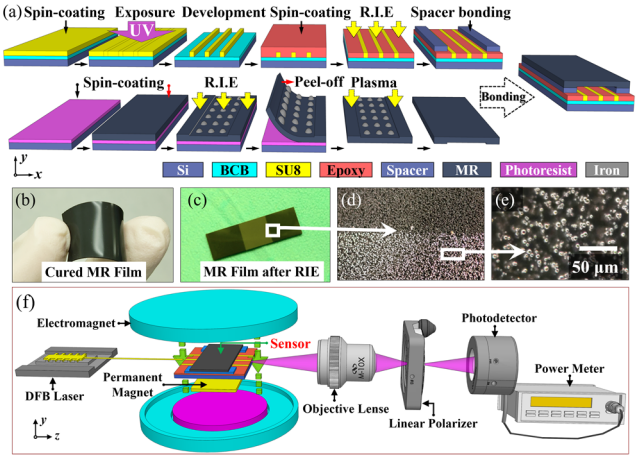

Fig. 4. (a) Fabrication process of proposed magnetic field sensor (b) Cured MR thin film sample with dark-grey appearance (c) MR thin film sample after RIE process to expose iron particles (d) and (e) Dark-field images of MR thin films at different magnifications; (f) Experimental setup for characterizing the sensing platform.

further scattering. Therefore, the transmission loss in region B depict signal saturation and it will not be suitable for sensing due to the limited dynamic sensing range.

The sensor fabrication includes the waveguide fabrication, MR film fabrication and their bonding, as depicted in Figure 4(a). The waveguide exhibits similar fabrication process as previous reports [10]. For the MR film, we firstly mixed the iron powder with uncured PDMS matrix by a weight ratio of 3:1. After degassing, the liquid mixture was spin coated onto a silicon wafer pre-coated by a layer of photoresist (SPR-6112B). This layer isolates the MR film with the wafer, thereby reducing the bonding energy to let the MR film easier peeling-off. After thermal curing, we obtained the MR film in Figure 4(b), where the MR film shows a shiny surface with dark-grey appearance. To activate a sensing region, a dry etching process was conducted to fully remove the PDMS covering the iron particles. As a result, the embedded particles will be exposed for evanescent scattering, leading to lighter color due to higher surface roughness as shown in Figure 4(c). Figures 4(d) and 4(e) compare the dark-field images of etched and unetched region, where the stronger light scattering confirms a good surface etching. After peeling-off, the MR film was bonded with the waveguide by a mechanical clamp at 75 °C for 2 hours. The index liquid was then dropped into the gap. Two sensor prototypes were fabricated with different MR film thickness of 210 μm (Sensor I) and 420 μm (Sensor II) for comparisons. Compares with optical MEMS, our fabrication process is simple and low cost, and also shows great potential of large-scale productions in industrial manufacturing.

Figure 4(f) illustrates the experimental setup fixed on a vibration free optical table for characterizing the sensing platform. A stablized light of 1.55 μm wavelength was coupled into the sensor by a single mode fiber via the end-fire coupling system. The power of TM polarization was captured by a power meter. To facilitate the magnetic sensing, an electromagnet was used to generate vertical magnetic flux (pre-calibrated by a Hall-effect gaussmeter, HT20, HTmagnet) to the MR film plane. The position of permanent magnet was carefully tuned by a micro-positioner to pre-bias the MR film by monitoring the output power. Alternation of Positive and Negative alignment was done by change direction of current flow in the coils. During the whole experiment, the

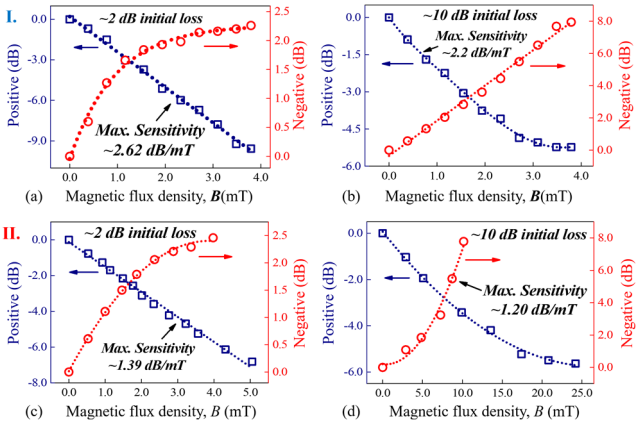

Fig. 5. Response of Sensor I at (a) Sensitive and (b) Saturation region; and Sensor II at (a) Sensitive and (b) Saturation region; blue: Positive alignment and red: Negative alignment.

environmental temperature was stabilized at 19.5 ± 0.5 °C to minimize the temperature crosstalk. To study the sensing response at different regions, we tune the PM to bias the MR film to two different initial positions, i.e. the initial loss of ~2 dB (Sensitive) and ~10 dB (Saturation), respectively.

In Figures 5(a) and 5(b), we present the normalized transmission loss versus the magnetic field *B* from 0 to 4.0 mT for Sensor I. From Figure 3(c), we read that Positive alignment (blue line) bends the film downward to increase the transmission loss, while Negative alignment (red line) reverses the film bending direction to weaken the evanescent scattering. Moreover, the signal linearity also relies on the bias position of MR film in the evanescent field [10]. For a Sensitive region in Figure 5(a), the transmission loss shows a quasi-linear response over a range of 4.0 mT in Positive alignment, where the maximum sensitivity was ~2.63 dB/mT. However, in Negative alignment, the optical power gradually recovered with a nonlinear response. The sensitivity is slightly lower than that of the Positive alignment due to less sensitive position of MR film. The experimental result indicates that the waveguide output shows different signal signs with respect to different field directions. Through this, our sensor can be used to distinguish magnetic polarity in real time. Figure 5(b) depicts the measurement result for the Saturation region. The Positive alignment (blue line) illustrates a quasi-linear response from 0 to 2.5 mT before turns saturation in $B \sim 4.0$ mT. In this case, the MR film has been sufficiently bent to a close vicinity to the waveguide surface, thereby showing gradual saturations. However, in Negative alignment (red line), MR film was pulled back to the sensitive region. Consequently, the sensor presents linear response, as indicated by the red line in Figure 5(b). The measured maximum sensitivity is ~2.2 dB/mT, which is comparable to the case of ~2 dB loss, since the MR film locates at similar positions.

Similarly, in Figures 5(c) and 5(d) we depict the normalized transmission loss versus magnetic flux density *B* for Sensor II. It is expected that with increase of film thickness, the displacement Δd would be reduced under the same magnetic field strength, thereby exhibiting lower sensitivity but larger dynamic sensing range. Figures 5(c) and 5(d) compare sensitivity performance for initial biasing positions at ~2 dB and ~10 dB loss, respectively. Similar to the Sensor I, Sensor II demonstrates similar response for an initial transmission loss of ~2 dB, where Positive alignment (blue line) shows a highly linear response while Negative alignment (red line) exhibits nonlinear response. In comparison with Sensor I, Sensor II achieves a maximum sensitivity of only ~1.39 dB/mT, which is lower than that of Sensor I as we expected. We further compare the response at ~10 dB initial loss in Figure 5(d). The Positive alignment (blue) generates a nonlinear scattering behavior with a much larger dynamic sensing range up to 25 mT. Similarly, the Negative alignment (red line) also depicts a nonlinear behavior, however, with slightly higher sensitivity (~1.20 dB/mT) than Positive alignment. This is due to negative field brings back the MR film back from saturation to the sensitive region. To compare two sensor prototypes, it turns out that Sensor I (thin sample) depicts higher sensitivity, however shorter dynamic sensing range than Sensor II (thick sample). This design flexibility would help to tune the sensing range in different applications.

We also present the stability check for Sensor I at Saturation region. The result reveals that our sensor exhibits excellent signal stability of standard deviation~0.044 dB over a span of 5 minutes. The fluctuation origins from laser power fluctuation and the environmental noise level like temperature and vibrations etc. The measured rise and fall time of Sensor II were about 750 ms, which can be potentially improved by using stiffer materials or with smaller sensor size. To compare with recent work in [5], our sensor depicts higher sensitivity, compact design and features in distinguishing magnetic polarities in real time.

In conclusion, we proposed a simple magnetic sensor that uses evanescent scattering by an MR film suspended above an optical waveguide. The film was to induce scattering on the evanescent field of a planar waveguide at proximity distance. This distance can be controlled precisely by the magnetic field. Consequently, the waveguide output power changes in response to the magnetic intensity. Two sensor prototypes with different film thickness were designed and compared. Experimental results indicate a trade-off between sensitivity and dynamic sensing range by varying the MR film thickness. A maximum sensitivity of ~2.62 dB/mT was achieved with an excellent signal stability ~0.044 dB . The sensor shows a moderate response time of ~750 ms, which can be possibly reduced by further geometric design and materials choices. The presented sensor features simple design, easy fabrication, low cost and high potential of large-scale production and sensor miniaturization into portable devices.

Funding. City University of Hong Kong (SRG-Fd 7004826).

Disclosures. The authors declare no conflicts of interest.

References

1. J. E. Lenz, P. IEEE **78**, 973 (1990).
2. O. Alem, R. Mhaskar, R. Jiménez-Martínez, D. Sheng, J. LeBlanc, L. Trahms, T. Sander, J. Kitching, and S. Knappe, Opt. Express **25,** 7849 (2017).
3. E. Udd, W. B. Spillman, John Wiley & Sons, 2011.
4. L. Sun, S. Jiang, and J. R. Marciante, Opt. Express **18,** 5407 (2010).
5. G. Violakis, N. Korakas, and S. Pissadakis, Opt. Lett. **43,** 142 (2018).
6. H. Wang, S. Pu, N. Wang, S. Dong, and J. Huang, Opt. Lett. **38**, 3765 (2013).
7. J. Dai, M. Yang, X. Li, H. Liu, and X. Tong, Opt. Fiber Technol. **17**, 210 (2011).
8. F. Keplinger, S. Kvasnica, A. Jachimowicz, F. Kohl, J. Steurer, and H. Hauser, Sensor Actuat. A-Phys. **110,** 112 (2004).
9. J. O. Dennis, F. Ahmad, M. Khir, N. H. B. Hamid, Sensors **15,** 18256 (2015).
10. B. Li, H. P. Chan, and K. T. Ahmmed, Opt. Express **8,** 12243 (2020).
11. B. Li, H. P. Chan, and K. T. Ahmmed, Opt. Lett. **43,** 5889 (2018).
12. J. R. Errigton, and D. A. Kofke, J. Chem. Phys. **127,** 174709 (2007).
13. B. Lee, P. Ravindra, and E. S. Chan, Chem. Eng. Commun. **195**, 889 (2008).

Full References

1. J. E. Lenz, “A review of magnetic sensors.” P. IEEE 78(6), 973-989 (1990).
2. O. Alem, R. Mhaskar, R. J. Martinez, D. Sheng, J. LeBlanc, L. Trahms, T. Sander, J. Kitching and S. Knappe, “Magnetic field imaging with microfabricated optically-pumped magnetometers.” Opt. Express 25(7), 7849-7858 (2017).
3. E. Udd and W. B. Spillman, “Fiber optic sensors: an introduction for engineers and scientists.” John Wiley & Sons, 2011.
4. L. Sun, S. Jiang and J. R. Marciante, “All-fiber optical magnetic-field sensor based on Faraday rotation in highly terbium-doped fiber.” Opt. Express 18(6), 5407-5412 (2010).
5. V. Georgios, N. Korakas and S. Pissadakis, “Differential loss magnetic field sensor using a ferrofluid encapsulated D-shaped optical fiber.” Opt. Lett. 43(1), 142-145 (2018).
6. H. Wang, S. Pu, N. Wang, S. Dong, J. Huang, “Magnetic field sensing based on singlemode–multimode–singlemode fiber structures using magnetic fluids as cladding.” Opt. Lett. 38 (19), 3765-3768 (2013).
7. J. Dai, M. Yang, X. Li, H. Liu, and X. Tong, “Magnetic field sensor based on magnetic fluid clad etched fiber Bragg grating.” Opt. Fiber Technol. 17(3), 210-213 (2011).
8. F. Keplinger, S. Kvasnica, A. Jachimowicz, F. Kohl, J. Steurer and H. Hauser, “Lorentz force based magnetic field sensor with optical readout.” Sensor Actua A- Phys. 110(1), 112-118 (2004).
9. J. O. Dennis, F. Ahmad, M. H. B. M. Khir and N. H. B. Hamid, “Optical characterization of lorentz force based CMOS-MEMS magnetic field sensor.” Sensors 15(8), 18256-18269 (2015).
10. B. Li, H. P. Chan and K. T. Ahmmed, “Investigation of evanescent scattering for low-distortion submicron vibration sensing using ferromagnetic cantilevers.” Opt. Express 28(8), 12243-12251 (2020).
11. B. Li, H. P. Chan and K. T. Ahmmed, “Precise control of evanescent scattering by self-assembled ferromagnetic particles for optical sensing with tunable sensitivity.” Opt. Lett. 43(23), 5889-5892 (2018).
12. J. R. Errington and D. A. Kofke, “Calculation of surface tension via area sampling.” J. Chem. Phys. 127(17), 174709 (2007).
13. B. B. Lee, P. Ravindra, and E. S. Chan, “A critical review: surface and interfacial tension measurement by the drop weight method.” Chem. Eng. Commun. 195(8), 889-924 (2008).